Journal of Materials Chemistry B

Accepted Manuscript

ROYAL SOCIETY OF CHEMISTRY

www.rsc.org/materialsB

Journal Name

RSCPublishing

ARTICLE

NIR excitation of upconversion nanohybrids containing a surface grafted Bodipy induces oxygen-mediated cancer cell death

Cite this: DOI: 10.1039/x0xx00000x

Received 00th January 2012,
Accepted 00th January 2012

DOI: 10.1039/x0xx00000x

www.rsc.org/

María González-Béjar,[1*] Marta Liras,[2†] Laura Francés-Soriano,[1] Valerio Voliani,[1] Vicente Herranz-Pérez,[3,4] Maria Duran-Moreno,[3,4] Jose M. Garcia-Verdugo,[3,4] Emilio I. Alarcon,[2] Juan C. Scaiano[1,2] and Julia Pérez-Prieto[1*]

We report the preparation of water-dispersible, ca. 30 nm-sized nanohybrids containing $NaYF_4$:Er^{3+},Yb^{3+} up-conversion nanoparticles (UCNPs), capped with a polyethylene glycol (PEG) derivative and highly-loaded with a singlet oxygen photosensitizer, specifically a diiodo-substituted Bodipy (IBDP). The photosensitizer, bearing a carboxylic group, was anchored to the UCNP surface and, at the same time, embedded in the PEG capping; the combined action of the UCNP surface and PEG facilitated the loading for an effective energy transfer and, additionally, avoided photosensitizer leaching from the nanohybrid (UCNP-IBDP@PEG). The effectiveness of the nanohybrids for generating singlet oxygen after near-infrared (NIR) excitation (975 nm) with a continuous wavelength (CW) laser was evidenced by using a probe molecule. In vitro assays demonstrated that the UCNP-IBDP@PEG nanohybrid was taken up by the SH-SY5Y human neuroblastoma-derived cells showing low cytotoxicity. Moreover, ca. 50% cancer cell death was observed after NIR irradiation (45 min, 239 mW).

Introduction

Photodynamic therapy (PDT) is a non-invasive cancer treatment that after selective delivery/administration of a photosensitizer (PS) uses light as an activator to produce reactive oxygen species for sequential cancer eradication. This therapy is beneficial when compared to chemotherapy and radiotherapy since it minimizes toxicity of healthy cells and side effects such as nauseas, vomiting, and immune-response.[1, 2] However, most of the photosensitizers lose photochemical activity and present limited cell-penetrating capacity due to their easy aggregation and poor solubility in aqueous solutions,[3] among them are photofrin,[4] methylene blue,[5] rose bengal,[6] Zn-phthalocyanines,[7, 8] and merocyanine 540.[9] Combination of photosensitizers (either via conjugation or complexation) with macromolecules, such as liposomes, lipids, and oligosaccharides, [1, 10-12] helps to deliver them. In addition, silica-based nanoparticles were recently developed to entrap water-insoluble photosensitizing agents and proved to be effective PDT drug carriers in aqueous media.[13, 14]

Multifunctional nanosystems that integrate multiple materials with different properties can provide new opportunities for simultaneous diagnosis and therapy of diseases. In this regard, the search for efficient PDT-photosensitizer/nanomaterial nanohybrids has been encouraging research in the last decade.[1] The application of magnetic nanoparticles,[15] optical down-converting nanoparticles, such as quantum dots[16] and metallic nanoparticles,[17-19] and photon up-converting nanoparticles[1] (UCNPs) is being explored as functional carriers of PDT-photosensitizers.

The so-called UCNPs are rare-earth fluoride nanocrystals, such $NaYF_4$, co-doped with trivalent lanthanides (such as Er, Yb, Tm) and are particularly relevant in the field of PDT[1, 14, 20-24] since they display good biocompatibility, narrow bandwidth, long-lived emission, high photostability, and no photoblinking.[25] Most importantly, they exhibit absorption in the near-infrared (NIR) which penetrates soft tissues to a greater extent than visible light,[1, 21, 26-29] and, consequently, induces minimum photodamage to living organisms and reduces auto-fluorescence background. Moreover, UCNPs can be excited with low-cost NIR continuous wave (CW) diode lasers which can be applied to illuminate large areas using low excitation energies and their emission wavelengths can be tuned as desired by selecting the co-doping lanthanide ratio.[29, 30] These interesting features make them useful for a large diversity of applications, among which bioimaging[21, 31-33] combines well with that of the photosensitizing capacity of UCNP-PS nanohybrids.[34] Comparatively, two-photon excited PDT also uses NIR light.[1] However, in this strategy, the photosensitizer (a photon down-converting PS) is excited by simultaneous absorption of two NIR low energy photons and requires the use of pulsed lasers as the light source to excite focused, small areas to obtain sufficient instantaneous energy to make the two-photon excitation possible.

There are several methods to make these UCNPs water-dispersible, such as coating them with silica[35, 36] or polymers.[37-42] Specifically, PS-embedded in silica-coated UCNPs (PS: $Ru(bpy)_3^{2+}$,[24] zinc phthalocyanine (ZnPc),[23, 35] merocyanine 540,[14] hypericin[43] and methylene blue[44]) have recently been reported in the context of singlet oxygen generation. In addition, rose bengal,[45] ZnPc,[46-48]

pyropheophorbide a[49], and chlorin e6 (Ce6)[41, 50] have been embedded in polymeric shells.

The drawbacks of some of these systems are the low PS payload and/or its leaching under experimental conditions. The high surface/volume ratio of the nanoparticles, combined with the capacity of their surface and ligands to establish stabilizing binding interactions with the PDT photosensitizer is an appealing strategy for improving the UCNP efficiency as a nanocarrier. Consequently, an ideal UCNP-PS nanohybrid for PDT would be a water-dispersible nanosystem with a large loading of a photosensitizer that exhibits a high capacity to generate reactive oxygen species (ROS), such as singlet oxygen, and is easily derivatized to incorporate a good anchoring group to the UCNP surface, thus making a considerable PS loading possible and, at the same time, avoiding leaching.

We report here the design and synthesis of β-$NaYF_4$:Yb^{3+}, Er^{3+} UCNPs carrying an efficient singlet oxygen photosensitizer, specifically a Bodipy derivative, anchored to its surface and embedded in the organic capping of the nanoparticle provided by a soft organic macromolecule such as a PEG derivative (Scheme 1). These nanoparticles, with a diameter of ca. 30 nm, bear a considerable loading of the Bodipy derivative, and are highly biocompatible in vitro. Their capacity for killing cancer cells after NIR excitation has been proven in an SH-SY5Y human neuroblastoma-derived cell line.

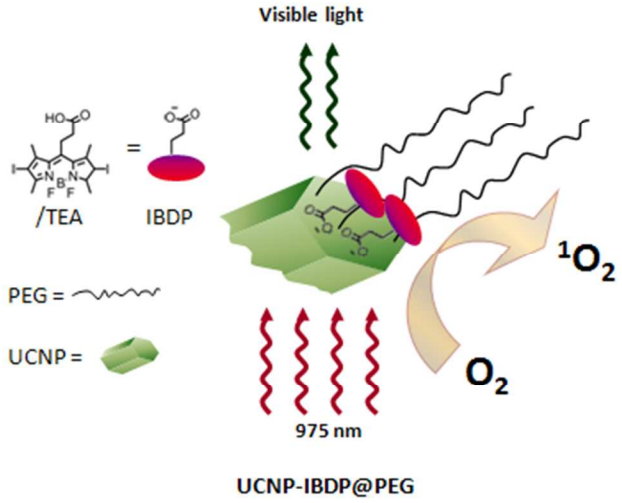

Scheme 1. Oversimplified image illustrating how UCNP@PEG (hexagonal nanoprism with polymeric shell) transfer their energy (wavy green arrows) to IBDP (pink ovals: see structure on the left) coordinated to the UCNP surface after being excited with a 975 nm CW diode. Triplet-triplet energy transfer from IBDP to oxygen leads to singlet oxygen generation.

Experimental

Materials

The chemicals used for the UCNP synthesis were: lanthanide chlorides ($YCl_3 \cdot 6H_2O$, $YbCl_3 \cdot 6H_2O$ and $ErCl_3 \cdot 6H_2O$ (>99.9%, all of them)), 1-octadecene (95%), oleic acid (99.9%), NaOH and NH_4F (99.99%). All chemicals were purchased from Sigma-Aldrich and used as received without previous purification. HS-PEG-NH_2 was purchased from Rapp-Polymere (3.0 kDa). 9,10-Anthracenediyl-bis(methylene)dimalonic acid (ABDA) was purchased from Aldrich. The synthesis of IBDP is described in the supporting information.

Synthesis of oleate-capped Up-converting $NaYF_4$:Yb^{3+}, Er^{3+} Nanoparticles: UCNP@oleate

$NaYF_4$:Yb, Er nanoparticles were synthesized following a previously reported protocol with some modifications.[51] Briefly, $YCl_3 \cdot 6H_2O$ (0.8 mmol), $YbCl_3 \cdot 6H_2O$ (0.18 mmol), and $ErCl_3 \cdot 6H_2O$ (0.02 mmol) were mixed with 12 mL oleic acid and 15 mL octadecene (ODE) in a 50 mL round-bottom Pyrex flask under continuous stirring. The solution was heated to 160 ºC. Once everything was dissolved, the mixture was cooled to 110 ºC. A 10 mL methanol solution containing NaOH (2.5 mmol) and NH_4F (4.0 mmol) was slowly added into the flask. The metal-oleate complexes in solution were stirred with a glass-coated magnetic stirring bar while being slowly heated to remove methanol, degassed at 100 ºC for 30 min, heated to 305 ºC and, finally, kept under N_2 flux during one hour. Then, the solution was cooled to room temperature and the nanoparticles were precipitated by centrifugation (10000 rpm, 10 min, 25 ºC). Later on, UCNP@oleate nanoparticles were washed three times with (43.5:40.5:16 v/v) hexane/acetone/methanol solution.

Synthesis of PEG-coated $NaYF_4$:Yb/Er up-converting nanoparticles: UCNP@PEG

These nanoparticles were prepared by using a method recently developed in our group.[40] A solution of UCNPs (10 mg) in degassed $CHCl_3$ (5 mL) was sonicated for 15 minutes. Then, 100 mg of HS-PEG-NH_2 were added. The solutions had 20 mg/mL of the hetero-functional PEG. The conjugation process was done in the presence of an excess of the PEG derivative.[37] The mix was kept in N_2 under strong stirring at 60 ºC overnight.

The opalescent solution was evaporated in vacuum and 5 mL of milliQ water were added. The dispersion was sonicated for 15 minutes. Then, 5 cycles of centrifugation at 10000 rpm x10 minutes with a total of 50 mL of acetonitrile were carried out in order to remove the oleate and PEG excess. The PEG-encapsulated UCNPs (UCNP@PEG) were resuspended in 1 mL of MilliQ water (or triethanolamine, TEA, 40 mM, pH 7.5) and stored at +4 ºC during one week maximum before their use.

Synthesis of UCNP-IBDP@PEG

The nanohybrids used in all the studies reported here (unless indicated) were prepared as follows: a solution of UCNP@PEG (300 µL, 10 mg/mL) in triethanolamine buffer (TEA, 40 mM, pH 7.5) was sonicated for 15 minutes and poured into a solution of 3-(2',6'-Diiodo-1',3',5',7'-tetramethyl-4',4'-difluoro-4'-bora-3'a,4'a-diaza-s-indacen-8'yl)propanoic acid (IBDP, 1.5 mg; UCNP@PEG/IBDP 1mg/0.5 mg ratio) in TEA (0.5 mg/mL). After stirring at RT for 24 h, the mixture was purified by centrifugation/sonication in acetonitrile (5 cycles of centrifugation for 10 minutes at 10000 rpm; sonication for 15 min). The nanohybrids (UCNP-IBDP@PEG) were re-suspended in 3 mL of milliQ water or TEA and stored at +4ºC.

Other UCNP-IBDP@PEG nanohybrids were prepared using different UCNP@PEG/IBDP weight ratios to determine the best IBDP loading for the ABDA photodegradation in the presence of oxygen (see Fig. S8 in the supporting information).

UV-Visible absorption measurements

All UV-Visible measurements were performed using an Agilent G1103A spectrometer equipped with quartz cuvettes. All samples were analyzed in milliQ water or buffer solutions.

Fluorescence and upconversion emission measurements

Upconversion emission spectra were collected by excitation at 975 nm using a CW 975 nm diode laser (Thorlabs L975P1WJ) as the excitation source coupled to the SLM Amingo Bowmann series 2 (AB2) fluorimeter (Microbeam, S.A.) and using a front-face set up.

Singlet oxygen quantum yield (Φ_Δ) calculations

The singlet oxygen phosphorescence decay traces were measured as follows: the aerated solutions placed in a 1 x 1 cm^2 fused silica cuvettes and capped with septa were irradiated at 532 nm with a laser (frequency doubled 532 nm, ~ 8 ns pulses, 12 mJ, from a Q-switched Nd/YAG laser 1064 nm). NIR emission studies[52] were carried out using a Peltier-cooled (-62.8˚C) Hamamatsu NIR detector (Model H10330-75) operating at 850 V coupled with a computer-controlled grating monochromator. A long pass filter, type FEL1150 filter from Thorlabs was placed in front of the monochromator. The photocurrent from the photomultiplier was stored on a digital oscilloscope (Tektronix TDS 2012). Signal rise times as short times (50 ns) were measured using the amplifier SR-445 from Stanford Research. Luzchem LFP software was used to acquire and process the data. All samples were measured under identical experimental conditions (same irradiation, day, and system alignment).

The amount of singlet oxygen generated was determined from phosphorescence decay curves in the NIR region by registering the phosphorescence decay data at 1270 nm. The singlet oxygen quantum yield is defined as the number of emitting $^1O_2$ molecules *per* photon absorbed by the photosensitizer. It has been estimated by using the ratio of slopes of linear plots of IBDP for the intensity of singlet oxygen phosphorescence (NIR excitation) against $1\text{-}10^{-A}$,[53] using a rose bengal (RB) solution in methanol as a standard, where A is the absorbance of the sample at the excitation wavelength. Different diluted solutions of IBDP and RB were prepared, such that their absorbance at the excitation wavelength (λ_{ex}= 532 nm) would be <0.40. Then the corresponding phosphorescence decay trace was recorded using this λ_{ex} and the quantum yield was obtained by:

$$\Phi_{IBDP} = \Phi_{RB} \frac{slope_{IBDP}}{slope_{RB}}$$

where RB stands for Rose Bengal used as a reference (Φ=0.76)[54] and IBDP stands for the corresponding BDP derivative. Φ are the corresponding singlet oxygen quantum yields.

Singlet oxygen Generation monitored by chemical photoconsumption of 9,10-anthracenediyl-bis(methylene)dimalonic acid (ABDA)

The samples were placed in quartz cuvettes (1x1 cm path length) and the emission was monitored in an AB2 Series spectrofluorimeter. All measurements were carried out in oxygen-saturated deuterium oxide solutions at room temperature. A similar method has been previously used to determine the ability of other UCNP-photosensitizers nanocomposites to generate singlet oxygen.[24, 35] The induced generation of singlet oxygen was estimated by measuring the decrease of ABDA fluorescence due to the formation of its endoperoxide. Briefly, a phosphate buffer solution (pH 7.2, 1.5 mL) containing 1 mg/mL of UCNP-IBDP@PEG and ABDA ($2x10^{-5}$ M) solution was prepared and kept under stirring. This solution was irradiated with a CW 975 nm diode laser of 138.5 mW in order to excite the UCNP-IBDP@PEG and generate singlet oxygen, and the ABDA emission (λ_{ex} = 380 nm) was recorded at different time intervals. For comparative purposes, a solution of ABDA ($2x10^{-5}$ M) in phosphate buffer was also irradiated under the same conditions. In addition, a control sample containing UCNP-IBDP@PEG and ABDA was kept in the dark (except when taking its fluorescence λ_{ex} = 380 nm, monitoring at 400 nm) at different time intervals.

Transmission electron microscopy (TEM)

Transmission electron microscopy (TEM) images were taken using a Jeol 1010 microscope operating at 100 kV equipped with a charge-coupled device (CCD) camera. High resolution TEM (HRTEM) and energy dispersive X-rays spectroscopy (EDX) were carried out by using a Field Emission Gun (FEG) TECNAI G2F20 microscope operated at 200 kV. Usually, for the preparation of the UCNP samples, 10 μL of a 0.5 mg/mL solution of the UCNPs was left to dry under air at room temperature on a formvar/carbon film supported on a 300 mesh copper grid.

Cytotoxicity assays

In vitro cytotoxicity was measured using a XTT Cell Proliferation Kit II (Roche, Mannheim, Germany) on SH-SY5Y cells (ATCC CRL-2266). Cells were seeded onto a 96-well plate at a density of $3 \cdot 10^4$ cells per well, under 100 % humidity, and were cultured at 37 °C and 5% CO_2 for 24 h; different concentrations of UCNP-IBDP@PEG (0, 25, 50, 100 and 250 μg/mL, diluted in culture medium) were then added to the wells. The cells were then incubated at 37 °C under 5% CO_2 for another 24 h.

The following day, XTT reagent (50 μL; 0.3 mg/mL) was added to each well and the plate was incubated at 37 °C under 5% CO_2 for 4 h. Then, the absorbance at 450 nm was measured with a standard scanning multi-well spectrophotometer (Thermo Scientific, Massachusetts, USA). Five replicates of each condition were carried out. The viability of untreated cells was assumed to be 100%, while relative viability of treated cells (%) was calculated using the formula shown bellow.

Photodynamic performance of neuroblastoma cells with UCNP-IBDP@PEG

SH-SY5Y cells were cultured in Dulbecco's modified Eagle medium/F-12 (DMEM/F-12) supplemented with 10% fetal bovine serum, 2mM L-glutamine, 50IU/mL penicillin, 50μg/mL streptomycin. SH-SY5Y cells were seeded onto 60 mm culture plates, allowed to incubate for 24 h at 37º C and then washed with PBS.

$$Cell\ viability(\%) = \frac{mean\ \text{of}\ A_{450}\ \text{value of treatment group}}{mean\ \text{of}\ A_{450}\ \text{value of control}} x100$$

A power-adjustable CW 975 nm diode laser (Thorlabs L975P1WJ) was collimated and used to irradiate the Petri dish. The output power was measured with a power-meter at the exact distance of the irradiation area (Thorlabs PM100A) and next, the cells were irradiated for 45 min. The Petri dish was kept at 37ºC while being irradiated.

Subsequently, cell viability was assessed by using Cell LIVE/DEAD® Kit (Life Technologies). Fluorescence was collected using a Zeiss Axiovert 40 CFL inverted microscope (Carl Zeiss AG, Oberkochen, Germany), in the 515-565 nm and 590–740 nm ranges for green (Calcein) and red (EthD1), respectively. Images were adjusted for brightness and contrast and analyzed with Fiji imaging software. Quantification was conducted by counting living *vs*. dead cells in the microscope's field located right in the center of the irradiated area (n = 3 replicates).

Additionally, in order to check cellular fine morphology cells were seeded on 4-well Permanox chamber slides (Nalgene Nunc International, Naperville, IL). Then, cells were irradiated as

described above and subsequently fixed in 3.5 % glutaraldehyde in 0.1 M phosphate buffer (PB) for 1 hour at 37 °C. Cells were post-fixed in 2% OsO_4 for 1 hour at room temperature and stained in 2% uranyl acetate in the dark for 2 h at 4 °C. Finally, cells were rinsed in distilled water, dehydrated in ethanol, and embedded overnight in Durcupan resin (Fluka, Sigma-Aldrich, St. Louis, USA). Following polymerization, serial semithin sections (1.5 µm) were cut with an UC-6 ultramicrotome (Leica, Heidelberg, Germany) and stained with 1% toluidine blue. Digital photomicrographs were acquired using a Nikon Eclipse E800 microscope. Ultrathin sections (60 – 70 nm) were also prepared and stained with lead citrate (Reynolds' solution). Finally, photomicrographs were obtained under a FEI Tecnai G^2 Spirit transmission electron microscope (FEI Europe, Eindhoven, Netherlands) using a Morada digital camera (Olympus Soft Image Solutions GmbH, Münster, Germany).

Results and discussion

Synthesis of β-NaYF4:Yb^{3+}, Er^{3+} UCNP coated with a PEG derivative and loaded with IBDP

Oleate capped β-$NaYF_4$:Yb^{3+}, Er^{3+} up-conversion nanoparticles (UCNP@oleate) were synthesized at high temperatures by using oleic acid and 1-octadecene as the organic capping ligand and a non-coordinating solvent, respectively.[51, 55, 56] The XRD pattern of the UCNP (Fig. S1) revealed the formation of the same pure hexagonal phase structure as bulk β-$NaYF_4$ (JCPDS 16-0334). The atomic ratios of lanthanides in the nanoparticles were obtained by energy-dispersive X-ray experiments (EDX) and were $NaYF_4$(81%):Yb^{3+}(16%), Er^{3+}(3%), see Fig. S2. Fig. 1 shows the transmission electron microscopy (TEM) and high-resolution TEM (HRTEM) images obtained for the monodisperse hexagonal nanoprisms together with the histogram that shows they had a uniform side length of approximately 16.1±1.4 nm, a height of 25.8±1.6 nm, and a base length of 18.0±1.4 nm. These nanoparticles stood or lay on the TEM grids as shown in Fig. 1A and Fig. 1C. The HRTEM shows the clear lattice fringes with a *d*-spacing of 0.52 nm (Fig. 1C). This is in accordance with the lattice spacing in (100) planes of hexagonal β-$NaYF_4$ and it is indicative of their high crystallinity.[48]

The coating of these particles made them hydrophobic thus, the UCNP@oleate were coated with a layer of bifunctional polyethylene glycol (HS-PEG-NH_2) following our recently reported protocol.[40] The layer of the soft organic macromolecules made the UCNPs water-dispersible without increasing significantly their size.[40] In fact, a polymeric shell thickness of about 2.5 ± 0.6 nm was evident in the TEM images of the PEG-coated UCNPs (UCNP@PEG), see Fig. 1D-E. In addition, capping of the UCNP with PEG is advantageous from the biological point of view, since it is non-toxic and prevents agglomeration and non-specific interactions with proteins and cells.[57]

The photosensitizer, 3-(2',6'-diiodo-1',3',5',7'-tetramethyl-4',4'-difluoro-4'-bora-3'a,4'a-diaza-s-indacen-8'yl)propanoic acid (IBDP, Scheme S1), is easily prepared[58] (see SI for experimental details) and exhibits high extinction coefficients in the visible region, in particular ca. 525 nm (molar extinction coefficient of 202 M^{-1} cm^{-1} at 525 nm), low probability of aggregation and resistance to photobleaching,[58-61] high triplet quantum yield, due to the internal heavy atom effect,[59, 62] and a good anchoring group to the UCNP, specifically a carboxylic group.

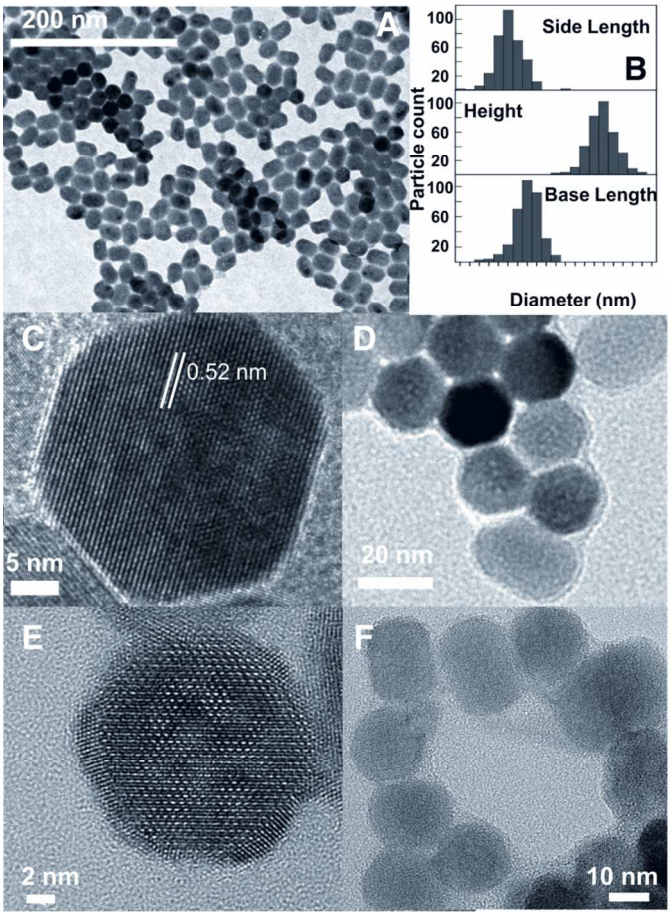

Fig. 1. (A) TEM images of UCNP@oleate nanoparticles. (B) Distribution of particle sizes of UCNP@oleate; mean size of 25.8 nm (height), and 16.1 nm (side length), and a base length of 18.0±1.4 nm. (C) HRTEM images of a hexagonal nanoprism of UCNP@oleate. (D) TEM image of UCNP@PEG with a shell thickness of 2.5 nm. (E) HRTEM images of UCNP@PEG. (F) HRTEM image of UCNP-IBDP@PEG.

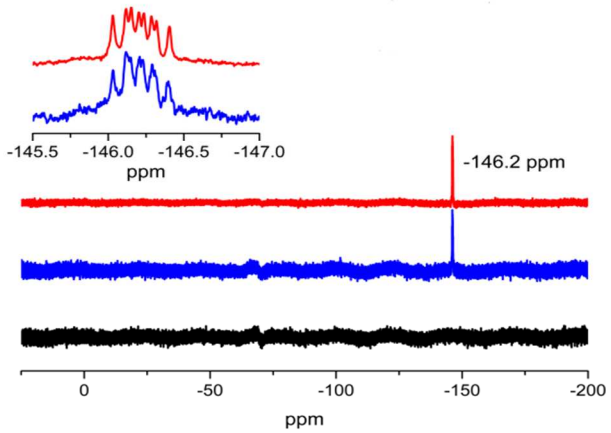

Fig. 2. ^{13}F-NMR of IBDP (top), UCNP-IBDP@PEG (middle) and UCNP@PEG (bottom) in $CDCl_3$.

Fig. S3 shows the pink colloidal solution of the nanoparticle obtained after adding IBDP to UCNP@PEG at pH = 7.5, followed by centrifugation and purification. The UV-Visible spectrum of this solution showed the incorporation of IBDP in the resulting UCNP (UCNP-IBDP@PEG), see Fig. S4. This was further corroborated by

^{19}F-NMR; thus, the spectrum of the UCNP-IBDP@PEG nanohybrids showed a signal at -146 ppm, ascribed to IBDP (Fig. 2).

The effectiveness in the IBDP loading was estimated from the UV-Vis absorption spectrum of UCNP-IBDP@PEG, by using the molar extinction coefficient of IBDP, and it tallied with TGA analysis (Fig. S5). Thus, values of 43% and 10% with respect to the UCNP core (*w*/*w*) were estimated for IBDP and the PEG, respectively. Examples of Bodipy aggregation are rare.[63] Consequently, we did not detect the formation of the IBDP dimers, which would absorb at lower and higher wavelengths than the monomer,[63] in the UV-Vis absorption spectrum of UCNP-IBDP@PEG nanohybrid in spite of the large cargo. The efficient PS loading is in accordance with the ability of the carboxylate groups to coordinate lanthanides[64] and offers advantages for PS loading.

The UCNP-IBDP@PEG nanohybrids proved to be stable in both water and PBS after keeping them in these media for three months. The stability of the nanohybrids was also checked in the cell culture medium (see experimental section). After one week in this medium, the nanohybrids were recovered by centrifugation while the supernatant remained practically colourless.

Control experiments showed the addition of IBDP to UCNP@oleate nanoparticles (under the same experimental conditions as those used with UCNP@PEG, i.e., basic conditions, UCNP/CH_3CN; TEA/IBDP) led to the precipitation of the nanoparticles as a pink solid. This confirmed that the UCNP@IBDP nanohybrids were not dispersible in the medium due to the limited solubility of the Bodipy moiety at the nanoparticle periphery. Attempts to suspend these nanoparticles in water were not fruitful, while the supernatant remained colorless. This suggests IBDP had become firmly grafted to the nanoparticle surface. In addition, this assay corroborated that PEG in the UCNP-IBDP@PEG nanohybrid played a key role for their water dispersibility. Moreover, under the same conditions, the addition of PM567, a Bodipy lacking the carboxylate group, to UCNP@oleate nanoparticles led to a white solid and a yellowish solution evidencing that most of the nanoparticles were centrifuged out while PM567 remained dissolved (UCNP/CH_3CN; TEA/PM567).

Capacity of the UCNP-IBDP@PEG nanohybrid for singlet oxygen generation

Fig. 3 shows the UV-Visible absorption spectrum of IBDP together with the upconversion luminescence spectra of UCNP@PEG and UCNP-IBDP@PEG in PBS upon 975 nm laser diode excitation. The UCNP@PEG emission spectrum exhibits an intense band at 540 nm ($^4S_{3/2}\rightarrow{}^4I_{15/2}$) with a small shoulder on the left ($^2H_{11/2}$, $^4S_{3/2}\rightarrow{}^4I_{15/2}$) and another at ca. 670 nm ($^4F_{3/2}\rightarrow{}^4I_{15/2}$).[65, 66] As expected from the overlap between the absorption spectrum of IBDP and the emission features of the UCNP@oleate, UCNP-IBDP@PEG excitation at 975 nm led to a quenching of the emission bands where IBDP absorbs (decrease of a 32% of the intensity in the 513-560 nm range), whereas the red emission was nearly unchanged. This quenching did not result in a new emission in the spectrum, as expected from the negligible fluorescence of IBDP (Φ_f= 0.02 in methanol).[59]

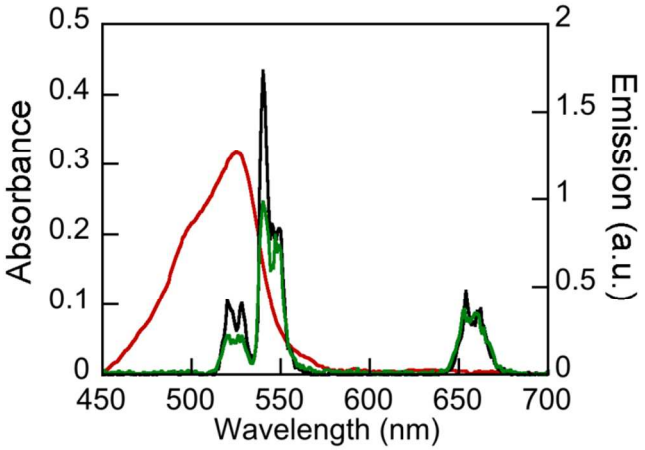

Fig. 3. IBDP (1.7 μM) UV-Visible absorption spectrum (red line) and luminescence emission spectra of solutions of UCNP@PEG (1mg/mL, black line) and UCNP-IBDP@PEG (1mg/mL, green line) in PBS.

The efficiency of IBDP for $^1O_2$ generation (Φ_Δ) was estimated as 0.61 in methanol by using RB as a standard (Φ_Δ = 0.76, see experimental and Fig. S6-S7). The effective generation of $^1O_2$ was also chemically demonstrated by using a singlet oxygen probe, specifically the disodium salt of 9,10-anthracenediyl-bis(methylene)dimalonic acid (ABDA).[35, 67] Thus, the formation of singlet oxygen after excitation at 975 nm of UCNP-IBDP@PEG in aqueous solution (D_2O) was assessed by measuring the decrease of the ABDA emission, a selective singlet oxygen trap, as function of the irradiation time using a 975 nm CW laser where only the UCNP core absorbs. Fig. 4 shows how the ABDA emission decreases with the exposure time of the nanohybrid to NIR, due to the formation of the corresponding, non-fluorescent ABDA endoperoxide. The data were fitted into an exponential decay function (rate constant for photobleaching of ADPA: k = 2.57 min^{-1}); this behaviour has been previously attributed to the probe quenching by the generated singlet oxygen.[14] The UCNP-IBDP@PEG proved highly efficient in ABDA bleaching, since the emission of the latter decreased in ca. 50% after only 15 min of NIR irradiation with low power. Comparatively, under the same conditions, the irradiation of ABDA in the absence and in the presence of UCNP@PEG showed no decrease of ABDA fluorescence in the same time-scale.

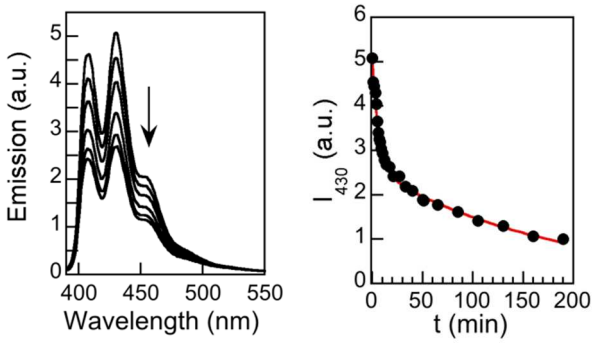

Fig. 4. Left: decrease in ABDA emission intensity overtime due to singlet oxygen emission generated by NIR excitation of the UCNP-IBDP@PEG nanohybrid in deuterated water (time intervals 0, 1, 4, 6, 10, 14 min). Right: decrease in the ABDA emission intensity registered at 430 nm for up to 200 min.

Scheme 1 shows a simplified representation for the process that would produce singlet oxygen upon NIR excitation of the UCNP-IBDP@PEG nanohybrid. The photophysical pathways that take place when this nanohybrid is excited with NIR light (975 nm) should be as follows. First, the upconversion process leads to the well-known erbium emissions. The IBDP derivative absorbs light from the $^4F_{7/2}$ and the $^2H_{11/2}$ erbium levels reaching its singlet-excited state that leads to its triplet excited state by intersystem crossing. Then, singlet oxygen is generated by triplet-triplet energy transfer from the IBDP triplet to oxygen in the ground state.

In vitro photocytotoxicity of UCNP-IBDP@PEG nanohybrids against cells

The UCNP-IBDP@PEG nanohybrid proved stable in PBS and cell culture medium and therefore, it further provided a suitable framework for biological applications. To corroborate this, human neuroblastoma SH-SY5Y cells were cultured at different concentrations of the nanohybrid in order to test their effect on cell proliferation. This was assessed by using an XTT-assay (Fig. S9). Cell viability of the control cells was assumed to be 100%. After 24 h incubation with UCNP-IBDP@PEG at 25 μg/mL, no effect on cell viability was measurable. When the concentration of the nanohybrid was increased to 50 μg/mL, cell viability dropped less than 10%. Only with a 250 μg/mL concentration, the toxicity of the nanohybrid was evident with a significant reduction of 40% in viable cells (n = 5; $P < 0.01$, Mann Whitney's "*U*" test). These safe working conditions in the 1-100 μg/mL range are in accordance with those published[68, 69] by others using other UCNPs derivatives and different cell types.[70] Further, at the highest 250 μg/mL condition irregular membranes, cellular aggregates, condensed nuclear chromatin and even picnotic cells were visible, as previously observed for the PEGylated UCNPs (data not shown).[40]

The uptake of UCNP-IBDP@PEG by SH-SY5Y cells, incubation with 10 μg/mL of the nanohybrid diluted in culture medium, was completed in 2 h. We were also able to detect cytoplasmic fluorescent signal in both the green and red emission spectra of the nanohybrid, highly co-localizing (Fig. S10), which proved that this nanohybrid could be used for simultaneous cell imaging and PDT.[45] This confirms that UCNP-IBDP@PEG nanohybrids were taken up by cells and maintained their photosensitive characteristics intracellularly.

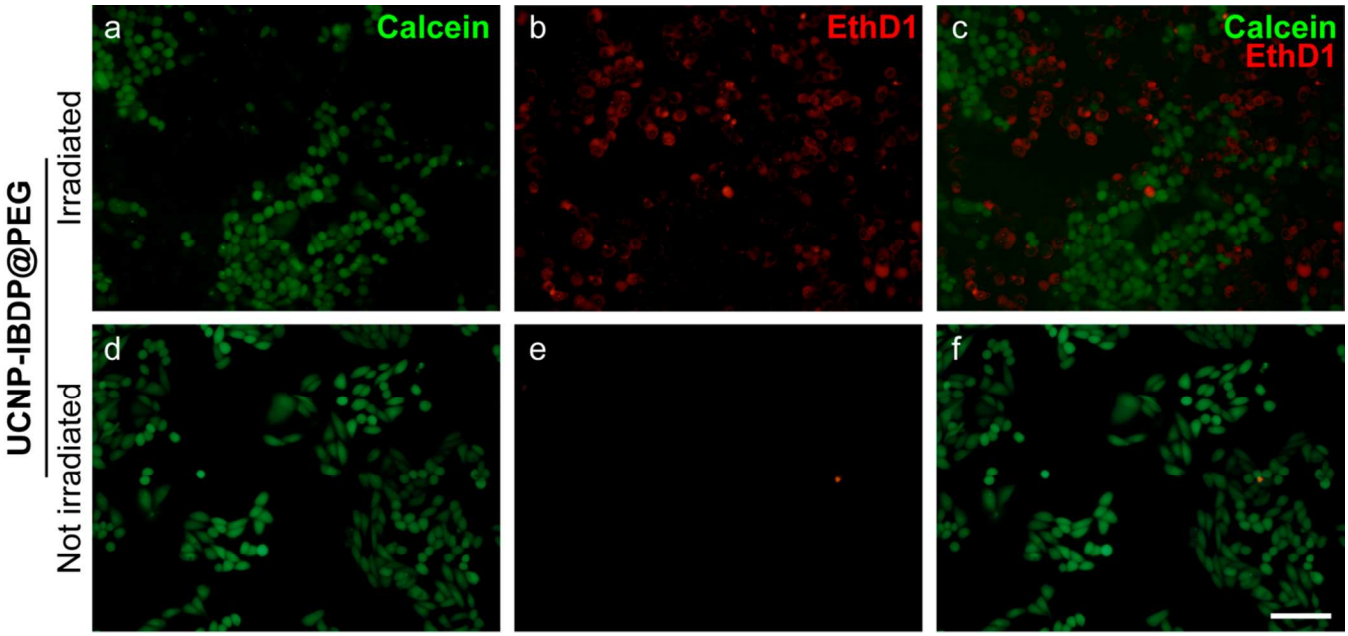

Fig. 5. SH-SY5Y cells incubated with UCNP-IBDP@PEG (A-F), were irradiated with a CW laser at 975 nm for 45 min. Cell viability was subsequently assayed with Life Technologies LIVE/DEAD® Kit. Cells with compromised membranes exhibit red-fluorescence from the live-cell impermeant nucleic acid stain ethidium homodimer-1 (λ_{ex}: 510-560 nm; λ_{em}: 590 nm). Cells with intact cell membranes are able to use nonspecific cytosolic esterases to convert nonfluorescent calcein AM into green-fluorescent calcein (λ_{ex}: 450-490 nm; λ_{em}: 515-565 nm.. No perceptible changes were detected out of the irradiation spot in either group (D-F). Scale bar = 100 μm.

Then, our experiments demonstrated the efficacy of the *in-vitro* PDT with the UCNP-IBDP@PEG nanohybrid, which led to destruction of SH-SY5Y human neuroblastoma cells. Here, cells incubated with UCNP-IBDP@PEG (25 μg/mL) were irradiated for 45 min with CW laser light operating at 975 nm with a total power of 239 mW, thus resulting in a 50.6 ± 3.2% cell mortality.

Our power is below 1 W and therefore suitable for clinical applications and most PDT experiments. After NIR exposure the components of the LIVE/DEAD® Kit were added to the Petri dish as described in the protocol. Cells with compromised membranes exhibit red-fluorescence from the live-cell–impermeant nucleic acid stain ethidium homodimer-1 (EthD1) whereas cells with intact cell membranes convert nonfluorescent calcein AM into bright green-fluorescent calcein by using nonspecific cytosolic esterases.[71-73]

It was determined that only NIR-irradiated cells were damaged whereas the non-irradiated cells remained intact (Fig. 5). Control experiments incubated with UCNP@PEG or in the absence of nanoparticles (Figure S10 A-F and G-L, respectively) did not show any cell death, thus proving that cell lethality is solely due to the irradiation of the UCNP-IBDP@PEG nanohybrid.

The human neuroblastoma SH-SY5Y cell line shows neuroblastic characteristics[74] and, thus, we presumed it would serve as a good

model to test our system *in vitro*. Consequently, we tested the potential use of this system for PDT. The mechanism of induced cell-death by cellular $^1O_2$ accumulation was first thought to be due to necrosis,[75, 76] but it was later found to be caused mainly by apoptotic processes. This was supported by the most relevant morphological and biochemical changes observed in cells subjected to oxygen radicals: chromatin condensation, membrane alteration, and mitochondrial swelling and apoptotic bodies. [23, 77]

To further investigate the underlying processes triggered by NIR light irradiation of UCNP-IBDP@PEG incubated cells, we seeded SH-SY5Y cells in 4-well chamber slides and irradiated a defined area of the well surface, while the rest of it remained completely out of the laser beam. We then obtained toluidine blue-stained semithin sections of the cell culture in order to appreciate the fine details of the cells (Fig. 6). We observed that the appearance of control cells was healthy, with no detectable differences between the irradiated and the non-irradiated cells (Fig. 6, A and B). Conversely, when the nanohybrid-incubated cells were irradiated, they showed abundant signs of cell damage when compared to their non-irradiated counterpart (Fig. 6, C and D).

These alterations included an increase in cytosolic vacuoles, swelling, irregular nuclear membranes and picnotic cells. When analyzed with electron microscopy, treated cells exhibited large masses of heterogeneous matter together with empty vacuole-like spaces (Fig. 6E). These structures measured up to 3 μm in diameter. Other cells presented smaller but more numerous masses. At higher magnification, UCNP-IBDP@PEG particles were detectable, highly electron-dense, in the periphery and within these structures (Fig. 6F). On occasions, membranous masses were also observed (Fig. 6G). Cytoplasmic vacuolization upon exposure to a variety of chemicals and bioactive substances has been extensively reported[78] and in our system it can be confidently attributed to singlet oxygen after NIR light irradiation.

It is essential to pursue new steps with the aim of maximizing PDT usefulness, since most studies report partial effectiveness inducing cancer cell death and with a discrepant homogeneity.[79] Also, it is crucial to improve the specificity of anti-tumoral treatments, especially when surrounded by extremely sensitive areas like the central nervous system. This is still more challenging due to tumoral cell heterogeneity.

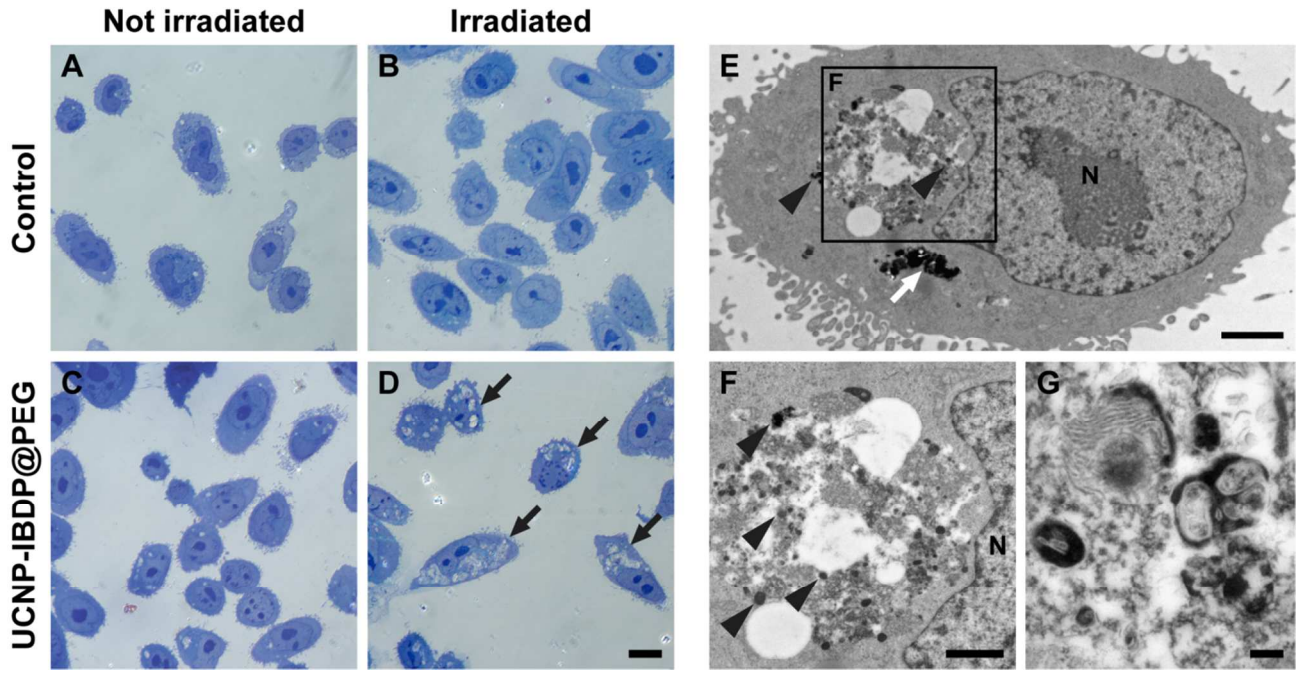

Fig. 6. Semithin and ultrathin sections of SH-SY5Y cells after irradiation with a 975 nm laser diode. Control (A-B) and UCNP-IBDP@PEG incubated cells (C-D) are compared in a NIR light irradiated zone and in a non-irradiated area of the same petri dish. The nanohybrid-treated cells of the irradiated area (D) show exceptionally large vacuoles (black arrows) and signs of cellular damage. In electron microscopy images (E-G) UCNP accumulations are detectable (E, white arrow), but also scattered single nanoparticles (arrowheads) within a masses of heterogeneous cellular matter. The rest of the cytoplasmic content and microvilli are well preserved. At higher magnification UCNPs are evident within the mass (F, arrowheads), which presents an heterogeneous appearance and severe vacuolization. This is the most frequent structure, although occasionally membranous structures are also found (G). A-D are toluidine blue-stained semithin sections, E-G are transmission electron microscopy images. N, nucleus. Scale bar: A-D = 10 μm; E = 2 μm; F = 1 μm; G = 200 nm.

Our UCNP-IBDP@PEG nanohybrid allows for additional functionalization since it still has the ability to bind covalently other PS by using the free terminal amino groups, which would make a higher loading possible (although a higher loading does not guarantee a better PDT efficiency)[46,50] The idea of PS co-loading using silica-coated UCNPs has been recently proven successful for PDT in vivo.[68] Alternatively, the free terminal amino groups would be of utmost importance for the addition of potential targeting ligands that provide specific nanoparticle-cell surface interactions, targeting nanoparticles to specific cancer cell membrane-receptor proteins. This facilitated guidance of ligands enhances cellular uptake into cancer cells, rather than increasing nanoparticle accumulation in the tumor's extracellular matrix.[80] For this reason, we think our system represents a good candidate for PDT, with additional uses for bioimaging and ability to bind specific ligands in order to improve cell specificity.

Conclusions

In summary, we have successfully developed an UCNP-IBDP@PEG nanohybrid comprising an upconversion nanoparticle core and a PEG shell, and IBDP chemisorbed to the UCNP core surface and, at the same time, embedded in the PEG capping. To our knowledge, this is the first time that a photosensitizer has been chemisorbed on the UCNP surface. This nanocomposite, of ca. 30-nm in diameter, acts as an efficient carrier of a considerable amount of the photosensitizer, it is dispersible in PBS and stable in the colloidal solution, and it generates reactive oxygen species after NIR excitation. These features make this nanohybrid an ideal candidate for PDT. The terminals on PEG chains are still available for conjugation with, for example, targeting ligands or other photosensitizer matching the absorption of the red emission of the UCNP (for complete use of upconversion energy to maximize PDT efficiency).

The UCNP-IBDP@PEG nanohybrid did not cause cell death in the standard cell culture conditions, and proved capable of effectively reducing the number of human neuroblastoma SH-SY5Y cells *in vitro*. Hence, it opens the way for their use in low-invasive tumoral phototherapy.

Acknowledgements

We thank Mr. Michel Grenier for his help with the laser diode and temperature control assembly and Arturo Prudencio (Mibrobeam, S.A.) for his help with the fluorimeter set-up and laser diode calibration. We thank the Spanish Ministry of Economy and Competitiveness (Project CTQ2011-27758, M.G.B Juan de la Cierva contract and L.F.S. FPU) and the University of Valencia (JCS for a visiting professorship) and the Fundació La Marató de TV3 (121730/31/32). This research was supported by a Marie Curie Career Integration Grants within the 7th European Community Framework Programme. The authors also thank NSERC and University of Ottawa for the generous financial support.

Notes and references

[a] Instituto de Ciencia Molecular / ICMOL, Universidad de Valencia, C/ José Beltrán 2, 46980, Paterna, Valencia, Spain.
[b] Department of Chemistry and Centre for Catalysis Research and Innovation, 10, Marie Curie, University of Ottawa, Ottawa, Ontario, K1N 6N5 Canada.
[d] Laboratorio de Neurobiología Comparada, Instituto Cavanilles de Biodiversidad y Biología Evolutiva, C/ Catedrático José Beltrán, 2, 46980 Paterna, Universidad de Valencia, CIBERNED, Valencia, Spain.
[e] Unidad mixta de Esclerosis múltiple y neurorregeneración, IIS Hospital La Fe, Valencia, Spain.
† Departamento de Química y Propiedades de Materiales Poliméricos, Instituto de Ciencia y Tecnología de Polímeros, CSIC, Juan de la Cierva 3, 28006 Madrid, Spain..
*E-mail: maria.gonzalez@uv.es; julia.perez@uv.es

Author contributions: The manuscript was written through contributions of all authors. All authors have given approval to the final version of the manuscript.

Abbreviations: UCNPs, up-conversion nanoparticles; PEG, polyethylene glycol; IBDP; PDT, photodynamic therapy; PS, photosensitizer; NIR, near-infrared; CW, continuous wave; ROS, reactive oxygen species; ABDA, Anthracenediyl-bis(methylene) dimalonic acid; TEA, triethanol amine; IBDP, Diiodo-1',3',5',7'-tetramethyl-4',4'-difluoro-4'-bora-3'a,4'a-diaza-s-indacen-8'yl)propanoic acid; Φ_Δ, singlet oxygen quantum yield; LFP, laser flash photolysis; RB, rose bengal; TEM, transmission electron microscopy; XRD, X-ray diffraction; EthD1, ethidium homodimer-1.

Electronic Supplementary Information (ESI) available: [XRD, EDX, synthesis of IBDP dyes, UCNP-IBDP@PEG absorption spectrum and TGA, plot for singlet oxygen quantum yield determination, singlet oxygen emission spectrum and phosphorescence decay at 1270 nm, control assays of SH-SY5Y cells incubated with UCNP@PEG or control medium, and confocal images of UCNP-IBDP@PEG incubated with SH-SY5Y cells]. See DOI: 10.1039/b000000x/

1. C. Wang, L. Cheng and Z. Liu, *Theranostics*, 2013, **3**, 317-330.
2. T. J. Dougherty, *Photochem. Photobiol.*, 1993, **58**, 895-900.
3. R. Ideta, F. Tasaka, W.-D. Jang, N. Nishiyama, G.-D. Zhang, A. Harada, Y. Yanagi, Y. TamakI, T. Aida and K. Kataoka, *Nano Lett.*, 2005, **5**, 2426-2431.
4. A. Roby, S. Erdogan and V. P. Torchilin, *Eur. J. Pharm. Biopharm.*, 2006, **62**, 235-240.
5. J. P. Tardivo, A. Del Glio, C. S. de Oliveira, D. S. Gabrielli, H. C. Junqueira, D. B. Tada, D. Severino, R. F. Turchiello and M. S. Baptista, *Photodiagn. Photodyn. Ther.*, 2005, **2**, 175-191.
6. D. C. Neckers, *J. Photochem. Photobiol. A: Chem.*, 1989, **47**, 1-29.
7. A. M. Garcia, E. Alarcon, M. Muñoz, J. C. Scaiano, A. M. Edwards and E. Lissi, *Photochem. Photobiol. Sci.* , 2011, **10**, 507-514.
8. G. Jori and C. Fabris, *J. Photochem. Photobiol. B: Biol.*, 2000, **43**, 181-185.
9. E. Alarcón, A. Aspée, M. González-Béjar, A. M. Edwards, E. Lissi and J. C. Scaiano, *Photochem. Photobiol. Sci.*, 2010, **9**, 861–869.
10. Y. Cheng, A. C. Samia, J. D. Meyers, I. Panagopoulos, B. Fei and C. Burda, *J. Am. Chem. Soc.*, 2008, **130**, 10643–10647.
11. Y. Cheng, J. D. Meyers, A.-M. Broome, M. E. Kenney, J. P. Basilion and C. Burda, *J. Am. Chem. Soc.*, 2011, **133**, 2583-2591.
12. M. González-Béjar, P. Montes-Navajas, H. García and J. C. Scaiano, *Langmuir*, 2009, **25**, 10490–10494.
13. I. Roy, T. Y. Ohulchanskyy, H. E. Pudavar, E. J. Bergey, A. R. Oseroff, J. Morgan, T. J. Dougherty and P. N. Prasad, *J. Am. Chem. Soc.*, 2003, **125**, 7860-7865.
14. P. Zhang, W. Steelant, M. Kumar and M. Scholfield, *J. Am. Chem. Soc.*, 2007, **129**, 4526-4527.
15. D. B. Tada, L. L. R. Vono, E. L. Duarte, R. Itri, P. K. Kiyohara, M. S. Baptista and L. M. Rossi, *Langmuir*, 2007, **23**, 8194-8199.
16. A. C. S. Samia, X. Chen and C. Burda, *J. Am. Chem. Soc.*, 2003, **125**, 15736-15737.
17. V. Voliani, G. Signore, O. Vittorio, P. Faraci, S. Luin, J. Peréz-Prieto and F. Beltram, *J. Mater. Chem. B*, 2013, **1**, 4225-4230.
18. E. C. Dreaden, M. A. Mackey, X. Huang, B. Kangy and M. A. El-Sayed, *Chem. Soc. Rev.*, 2011, **40**, 3391–3404
19. Y. Zhang, K. Aslan, M. J. R. Previte, S. N. Malyn and C. D. Geddes, *J. Phys. Chem. B*, 2006, **110**, 25108-25114.
20. B. Ungun, R. K. Prud'homme, S. J. Budijono, J. Shan, S. F. Lim, Y. Ju and R. Austin, *Opt. Express*, 2009, **17**, 80-86.
21. F. Wang, D. Banerjee, Y. Liu and X. C. X. Liu, *Analyst*, 2010, **135**, 1839–1854.
22. C. Li and J. Lin, *J. Mater. Chem.*, 2010, **20**, 6831-6847.
23. H. Guo, H. Qian, N. M. Idris and Y. Zhang, *Nanomedicine*, 2010, **6**, 486–495.

24. Y. Guo, M. Kumar and P. Zhang, *Chem. Mater.*, 2007, **19**, 6071–6072.
25. S. Wu, G. Hana, D. J. Millirona, S. Alonia, V. Altoea, D. V. Talapin, B. E. Cohena and P. J. Schuck, *Proc. Natl. Acad. Sci. U.S.A.*, 2009, **106**, 10917-10921.
26. J. C. G. Bünzil and S. V. Eliseeva, *Chem. Sci.*, 2013, **4**, 1939-1949.
27. N. Menyuk, K. Dwight and J. W. Pierce, *Appl. Phys. Lett.*, 1972, **21**, 159-162.
28. J.-C. Boyer, C.-J. Carling, B. D. Gates and N. R. Branda, *J. Am. Chem. Soc.*, 2010, **132**, 15766–15772.
29. Z. Li, Y. Zhang and S. Jiang, *Adv. Mater.*, 2008, **20**, 4765-4769.
30. F. Wang and X. Liu, *J. Am. Chem. Soc.*, 2008, **130**, 5642–5643.
31. S. F. Lim, R. Riehn, W. S. Ryu, N. Khanarian, C.-k. Tung, D. Tank and R. H. Austin, *Nano Lett.*, 2006 **6**, 169-174.
32. R. Kumar, M. Nyk, T. Y. Ohulchanskyy, C. A. Flask and P. N. Prasad, *Adv. Funct. Mater.*, 2009, **19**, 853–859.
33. K. König, *J. Microsc.*, 2000, **200**, 83-104.
34. C. Li, Z. Hou, Y. Dai, D. Yang, Z. Cheng, P. a. Ma and J. Lin, *Biomater. Sci.*, 2013, **1**, 213-223.
35. H. S. Qian, H. C. Guo, P. C.-L. Ho, R. Mahendran and Y. Zhang, *Small*, 2009, **5**, 2285–2290.
36. R. A. Jalil and Y. Zhanga, *Biomaterials*, 2008, **29**, 4122–4128.
37. J.-C. Boyer, M.-P. Manseau, J. I. Murray and F. C. J. M. v. Veggel, *Langmuir* 2010, **26**, 1157–1164
38. F. Wang, D. V. Chatterjee, Z. Li, Y. Zhang, X. Fan and M. Wang, *Nanotechnology*, 2006, **17**, 5786-5791.
39. N. J. J. Johnson, N. M. Sangeetha, J.-C. Boyer and F. C. J. M. v. Veggel, *Nanoscale*, 2010, **2**, 771–777.
40. V. Voliani, M. González-Béjar, V. Herranz-Pérez, M. Duran-Moreno, G. Signore, J. M. Garcia-Verdugo and J. Pérez-Prieto, *Chem. Eur. J.*, 2013, **19**, 13538-13546.
41. C. Wang, L. Cheng and Z. Liu, *Biomaterials*, 2011, **32**, 6145-6154.
42. J. Jin, Y.-J. Gu, C. W.-Y. Man, J. Cheng, Z. Xu, Y. Zhang, H. Wang, V. H.-Y. Lee, S. H. Cheng and W.-T. Wong, *ACS Nano*, 2011, **5**, 7838-7847.
43. X. Yang, Q. Xiao, C. Niu, N. Jin, J. Ouyang, X. Xiao and D. He, *J. Mater. Chem. B*, 2013, **1**, 2757–2763.
44. F. Chen, S. Zhang, W. Bu, Y. Chen, Q. Xiao, J. Liu, H. Xing, L. Zhou, W. Peng and J. Shi, *Chem. Eur. J.*, 2012, **18**, 7082-7090.
45. K. Liu, X. Liu, Q. Zeng, Y. Zhang, L. Tu, T. Liu, X. Kong, Y. Wang, F. Cao, S. A. G. Lambrechts, M. C. G. Aalders and H. Zhang, *ACS Nano*, 2012, **6**, 4054-4062.
46. S. Cui, D. Yin, Y. Chen, Y. Di, H. Chen, Y. Ma, S. Achilefu and Y. Gu, *ACS Nano*, 2013, **7**, 676-688.
47. S. Cui, H. Chen, H. Zhu, J. Tian, X. Chi, Z. Qian, S. Achilefuc and Y. Gu, *J. Mater. Chem.*, 2012, **22**, 4861-4873.
48. Q. Xiao, Y. Ji, Z. Xiao, Y. Zhang, H. Lin and Q. Wang, *Chem. Commun.*, 2013, **49**, 1527-1529.
49. A. Zhou, Y. Wei, B. Wu, Q. Chen and D. Xing, *Mol. Pharmaceutics*, 2012, **9**, 1580-1589.
50. Y. I. Park, H. M. Kim, J. H. Kim, K. C. Moon, B. Yoo, K. T. Lee, N. Lee, Y. Choi, W. Park, D. Ling, K. Na, W. K. Moon, S. H. Choi, H. S. Park, S.-Y. Yoon, Y. D. Suh, S. H. Lee and T. Hyeon, *Adv. Mater.*, 2012, **24**, 5755-5761.
51. Z. Li and Y. Zhang, *Nanotechnology*, 2008, **19**, 345606-345610.
52. B. Cojocaru, Laferrière, M., Carbonell, E., Parvulescu, V., García, H., Scaiano, J. C., *Langmuir*, 2008, **24**, 4478-4481.
53. E. Oliveros, S. H. Bossman, S. Nonell, C. Martí, G. Heit, G. Tröscher, A. Neuner, C. Martínez and A. M. Braun, *New. J. Chem.*, 1999, **23**, 85-93.
54. K. Gollnick, T. Franken, M. F. R. Fouda, H. R. Paur and S. Held, *J. Photochem. Photobiol. B: Biol.*, 1992, **12**, 57-81.
55. H.-X. Mai, Y.-W. Zhang, R. Si, Z.-G. Yan, L.-d. Sun, L.-P. You and C.-H. Yan, *J. Am. Chem. Soc.*, 2006, **128**, 6426-6436.
56. V. F. Boyer J-C, Cuccia L A, Capobianco J A, *J. Am. Chem. Soc.*, 2006, **128**, 7444-7445.
57. X. Xia, M. Yang, Y. Wang, Y. Zheng, Q. Li, J. Chen and Y. Xia, *ACS Nano*, 2011, **6**, 512-522.
58. S. Hui Lim, C. Thivierge, P. Nowak-Sliwinska, J. Han, H. van den Bergh, G. Wagnières, K. Burgess and H. B. Lee, *J. Med. Chem.*, 2010, **53**, 2865–2874.
59. T. Yogo, Y. Urano, Y. Ishitsuka, F. Maniwa and T. Nagano, *J. Am. Chem. Soc.*, 2005, **127**, 12162-12163.
60. S. Erbas, A. Gorgulu, M. Kocakusakogullaric and E. U. Akkaya, *Chem. Commun.*, 2009, 4956–4958.
61. N. Adarsh, R. R. Avirah and D. Ramaiah, *Org. Lett.*, 2010, **12**, 5720-5723.
62. M. J. Ortiz, A. R. Agarrabeitia, G. Duran-Sampedro, J. Bañuelos Prieto, T. Arbeloa Lopez, W. A. Massad, H. A. Montejano, N. A. García and I. Lopez Arbeloa, *Tetrahedron*, 2012, **68**, 1153-1162.
63. R. París, I. Quijada-Garrido, O. García and M. Liras, *Macromolecules*, 2011, **44**, 80-86.
64. M. Ottonelli, G. Musso and G. Dellepiane, *J. Phys. Chem. A*, 2008, **112**, 11960-11964.
65. J.-C. Boyer, F. Vetrone, L. A. Cuccia and J. A. Capobianco, *J. Am. Chem. Soc.*, 2006, **128**, 7444-7445.
66. F. Auzel, *Chem. Rev.*, 2004, **104**, 139−173
67. N. A. Kuznetsova, N. S. Gretsova, O. A. Yuzhakova, V. M. Negrimovskii, O. L. Kaliya and E. A. Luk'yanets, *Russ. J. Gen. Chem.*, 2001, **71**, 36-41.
68. N. M. Idris, M. K. Gnanasammandhan, J. Zhang, P. C.-L. Ho, R. Mahendran and Y. Zhang, *Nature Med.*, 2012, **18**, 1580-1585.
69. M. Nyk, R. Kumar, T. Y. Ohulchansky, E. J. Bergey and P. N. Prasad, *Nano Lett.*, 2008, **8**, 3834-3838.
70. C. Wang, L. Cheng, H. Xu and Z. Liu, *Biomaterials*, 2012, **33**, 4872-4881.
71. A. W. Hayes, 1994.
72. N. G. Papadopoulos, G. V. Z. Dedoussis, G. Spanakos, A. D. Gritzapis, B. C. N. and M. Papamichail, *J. Immunol. Methods.*, 1994, **177**, 101-111.
73. E. S. Kaneshiro, M. A. Wyder, Y.-P. Wu and M. T. Cushion, *J. Microbiol. Methods*, 1993, **17**, 1-16.
74. M. C. Lee, B. W. Kim, J. S. Kim, J. S. Lee, K. S. Kim, J. H. Lee, J. H. Nam, S. M. Rowe and S. U. Kim, *Brain Tumor Pathol.*, 1997, **14**, 5-11.
75. J. Moan and K. Berg, *Photochem. Photobiol.*, 1992, **55**, 931-948.
76. B. W. Henderson and T. J. Dougherty, *Photochem. Photobiol.*, 1992, **55**, 145-157.
77. M. L. Agarwal, M. E. Clay, E. J. Harvey, H. H. Evans, A. R. Antunez and N. L. Oleinick, *Cancer Res.*, 1991, **51**, 5993-5996.

78. T. Aki, A. Nara and K. Uemura, *Cell. Biol. Toxicol.* , 2012, **28**, 125-131.
79. E. C. Costa, V. M. Gaspar, J. G. Marques, P. Coutinho and I. J. Correia, *PLoS ONE*, 2013, **8**, e70072.
80. M. E. Davis, Z. Chen and D. M. Shin, *Nature Rev.*, 2008, **7**, 771-782.

A nanohybrid comprising a diiodo-substituted Bodipy anchored to the surface of $NaYF_4:Er^{3+},Yb^{3+}$ nanoparticles showed effective in inducing cancer cell death under NIR irradiation.

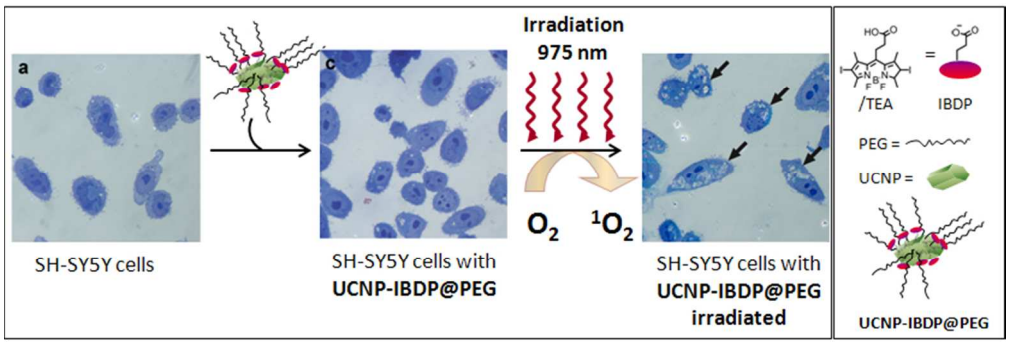

220x75mm (96 x 96 DPI)